Research Article | Vol. 8, No. 10 | 1 Oct 2017 | BIOMEDICAL OPTICS EXPRESS 4652
Biomedical Optics EXPRESS

Optophysiology of cardiomyocytes: characterizing cellular motion with quantitative phase imaging

CHRISTINE CORDEIRO,[1,*] OSCAR J. ABILEZ,[2,3] GEORGES GOETZ,[4] TUSHAR GUPTA,[1] YAN ZHUGE,[5] OLAV SOLGAARD,[1] AND DANIEL PALANKER[6,7]

[1]*Department of Electrical Engineering, Stanford University, Stanford, CA, 94305, USA*
[2]*Division of Cardiovascular Medicine, Stanford University, Stanford, CA, 94305, USA*
[3]*Cardiovascular Institute, Stanford University, Stanford, CA 94305, USA*
[4]*Department of Neurosurgery, Stanford University, Stanford, CA, 94305, USA*
[5]*Molecular Imaging Program at Stanford, Stanford University, Stanford, CA, 94305, USA*
[6]*Department of Ophthalmology, Stanford University, Stanford, CA, 94305, USA*
[7]*Hansen Experimental Physics Laboratory, Stanford University, Stanford, CA, 94305, USA*
[*]*c.cordeiro@stanford.edu*

Abstract: Quantitative phase imaging enables precise characterization of cellular shape and motion. Variation of cell volume in populations of cardiomyocytes can help distinguish their types, while changes in optical thickness during beating cycle identify contraction and relaxation periods and elucidate cell dynamics. Parameters such as characteristic cycle shape, beating frequency, duration and regularity can be used to classify stem-cell derived cardiomyocytes according to their health and, potentially, cell type. Unlike classical patch-clamp based electrophysiological characterization of cardiomyocytes, this interferometric approach enables rapid and non-destructive analysis of large populations of cells, with longitudinal follow-up, and applications to tissue regeneration, personalized medicine, and drug testing.

OCIS codes: (180.3170) Interference microscopy; (100.2960) Image analysis; (170.1530) Cell analysis.

References and links

1. I. Y. Chen, E. Matsa, and J. C. Wu, "Induced pluripotent stem cells: at the heart of cardiovascular precision medicine," Nat. Rev. Cardiol. **13**(6), 333–349 (2016).
2. M. Ben-Ari, S. Naor, N. Zeevi-Levin, R. Schick, R. Ben Jehuda, I. Reiter, A. Raveh, I. Grijnevitch, O. Barak, M. R. Rosen, A. Weissman, and O. Binah, "Developmental changes in electrophysiological characteristics of human-induced pluripotent stem cell-derived cardiomyocytes," Heart Rhythm **13**(12), 2379–2387 (2016).
3. X. Yang, L. Pabon, and C. E. Murry, "Engineering Adolescence: Maturation of Human Pluripotent Stem Cell-Derived Cardiomyocytes," Circ. Res. **114**(3), 511–523 (2014).
4. S. Peng, A. E. Lacerda, G. E. Kirsch, A. M. Brown, and A. Bruening-Wright, "The action potential and comparative pharmacology of stem cell-derived human cardiomyocytes," J. Pharmacol. Toxicol. Methods **61**(3), 277–286 (2010).
5. E. G. Navarrete, P. Liang, F. Lan, V. Sanchez-Freire, C. Simmons, T. Gong, A. Sharma, P. W. Burridge, B. Patlolla, A. S. Lee, H. Wu, R. E. Beygui, S. M. Wu, R. C. Robbins, D. M. Bers, and J. C. Wu, "Screening Drug-Induced Arrhythmia [corrected] Using Human Induced Pluripotent Stem Cell-Derived Cardiomyocytes and Low-Impedance Microelectrode Arrays," Circulation **128**(11 Suppl 1), S3–S13 (2013).
6. T. Hayakawa, T. Kunihiro, T. Ando, S. Kobayashi, E. Matsui, H. Yada, Y. Kanda, J. Kurokawa, and T. Furukawa, "Image-based evaluation of contraction-relaxation kinetics of human-induced pluripotent stem cell-derived cardiomyocytes: Correlation and complementarity with extracellular electrophysiology," J. Mol. Cell. Cardiol. **77**, 178–191 (2014).
7. N. Smedemark-Margulies and J. G. Trapani, "Tools, methods, and applications for optophysiology in neuroscience," Front. Mol. Neurosci. **6**, 18 (2013).
8. R. Shinnawi, I. Huber, L. Maizels, N. Shaheen, A. Gepstein, G. Arbel, A. J. Tijsen, and L. Gepstein, "Monitoring Human-Induced Pluripotent Stem Cell-Derived Cardiomyocytes with Genetically Encoded Calcium and Voltage Fluorescent Reporters," Stem Cell Rep. **5**(4), 582–596 (2015).
9. J. S. Leyton-Mange, R. W. Mills, V. S. Macri, M. Y. Jang, F. N. Butte, P. T. Ellinor, and D. J. Milan, "Rapid Cellular Phenotyping of Human Pluripotent Stem Cell-Derived Cardiomyocytes using a Genetically Encoded Fluorescent Voltage Sensor," Stem Cell Rep. **2**(2), 163–170 (2014).

#301837 https://doi.org/10.1364/BOE.8.004652
Journal © 2017 Received 10 Jul 2017; revised 15 Sep 2017; accepted 19 Sep 2017; published 22 Sep 2017

Biomedical Optics EXPRESS

10. T. J. Herron, P. Lee, and J. Jalife, "Optical Imaging of Voltage and Calcium in Cardiac Cells & Tissues," Circ. Res. **110**(4), 609–623 (2012).
11. M. Maddah, J. D. Heidmann, M. A. Mandegar, C. D. Walker, S. Bolouki, B. R. Conklin, and K. E. Loewke, "A non-invasive platform for functional characterization of stem-cell-derived cardiomyocytes with applications in cardiotoxicity testing," Stem Cell Rep. **4**(4), 621–631 (2015).
12. A. Ahola, A. L. Kiviaho, K. Larsson, M. Honkanen, K. Aalto-Setälä, and J. Hyttinen, "Video image-based analysis of single human induced pluripotent stem cell derived cardiomyocyte beating dynamics using digital image correlation," Biomed. Eng. Online **13**(1), 39 (2014).
13. N. Huebsch, P. Loskill, M. A. Mandegar, N. C. Marks, A. S. Sheehan, Z. Ma, A. Mathur, T. N. Nguyen, J. C. Yoo, L. M. Judge, C. I. Spencer, A. C. Chukka, C. R. Russell, P. L. So, B. R. Conklin, and K. E. Healy, "Automated Video-Based Analysis of Contractility and Calcium Flux in Human-Induced Pluripotent Stem Cell-Derived Cardiomyocytes Cultured over Different Spatial Scales," Tissue Eng. Part C Methods **21**(5), 467–479 (2015).
14. F. Zernike, "Phase contrast, a new method for the microscopic observation of transparent objects," Physica **9**(7), 686–698 (1942).
15. N. T. Shaked, L. L. Satterwhite, N. Bursac, and A. Wax, "Whole-cell-analysis of live cardiomyocytes using wide-field interferometric phase microscopy," Biomed. Opt. Express **1**(2), 706–719 (2010).
16. B. Bhaduri, D. Wickland, R. Wang, V. Chan, R. Bashir, and G. Popescu, "Cardiomyocyte imaging using real-time spatial light interference microscopy (SLIM)," PLoS One **8**(2), e56930 (2013).
17. B. Rappaz, I. Moon, F. Yi, B. Javidi, P. Marquet, and G. Turcatti, "Automated multi-parameter measurement of cardiomyocytes dynamics with digital holographic microscopy," Opt. Express **23**(10), 13333–13347 (2015).
18. D. Roitshtain, L. Wolbromsky, E. Bal, H. Greenspan, L. L. Satterwhite, and N. T. Shaked, "Quantitative phase microscopy spatial signatures of cancer cells," Cytometry A **91**(5), 482–493 (2017).
19. L. Kastl, M. Isbach, D. Dirksen, J. Schnekenburger, and B. Kemper, "Quantitative phase imaging for cell culture quality control," Cytometry A **91**(5), 470–481 (2017).
20. V. L. Calin, M. Mihailescu, E. I. Scarlat, A. V. Baluta, D. Calin, E. Kovacs, T. Savopol, and M. G. Moisescu, "Evaluation of the metastatic potential of malignant cells by image processing of digital holographic microscopy data," FEBS Open Bio (2017).
21. H. Byun, T. R. Hillman, J. M. Higgins, M. Diez-Silva, Z. Peng, M. Dao, R. R. Dasari, S. Suresh, and Y. Park, "Optical measurement of biomechanical properties of individual erythrocytes from a sickle cell patient," Acta Biomater. **8**(11), 4130–4138 (2012).
22. N. T. Shaked, L. L. Satterwhite, M. J. Telen, G. A. Truskey, and A. Wax, "Quantitative microscopy and nanoscopy of sickle red blood cells performed by wide field digital interferometry," J. Biomed. Opt. **16**(3), 030506 (2011).
23. S. A. Yang, J. Yoon, K. Kim, and Y. Park, "Measurements of morphological and biophysical alterations in individual neuron cells associated with early neurotoxic effects in Parkinson's disease," Cytometry A **91**(5), 510–518 (2017).
24. H. Park, S. Lee, M. Ji, K. Kim, Y. Son, S. Jang, and Y. Park, "Measuring cell surface area and deformability of individual human red blood cells over blood storage using quantitative phase imaging," Sci. Rep. **6**(1), 34257 (2016).
25. B. Bhaduri, H. Pham, M. Mir, and G. Popescu, "Diffraction phase microscopy with white light," Opt. Lett. **37**(6), 1094–1096 (2012).
26. M. Mir, Z. Wang, Z. Shen, M. Bednarz, R. Bashir, I. Golding, S. G. Prasanth, and G. Popescu, "Optical measurement of cycle-dependent cell growth," Proc. Natl. Acad. Sci. U.S.A. **108**(32), 13124–13129 (2011).
27. C. Edwards, B. Bhaduri, T. Nguyen, B. G. Griffin, H. Pham, T. Kim, G. Popescu, and L. L. Goddard, "Effects of spatial coherence in diffraction phase microscopy," Opt. Express **22**(5), 5133–5146 (2014).
28. B. Bhaduri, C. Edwards, H. Pham, R. Zhou, T. H. Nguyen, L. L. Goddard, and G. Popescu, "Diffraction phase microscopy: principles and applications in materials and life sciences," Adv. Opt. Photon. **6**(1), 57–119 (2014).
29. H. V. Pham, C. Edwards, L. L. Goddard, and G. Popescu, "Fast phase reconstruction in white light diffraction phase microscopy," Appl. Opt. **52**(1), A97–A101 (2013).
30. P. W. Burridge, E. Matsa, P. Shukla, Z. C. Lin, J. M. Churko, A. D. Ebert, F. Lan, S. Diecke, B. Huber, N. M. Mordwinkin, J. R. Plews, O. J. Abilez, B. Cui, J. D. Gold, and J. C. Wu, "Chemically defined generation of human cardiomyocytes," Nat. Methods **11**(8), 855–860 (2014).
31. D. Dussault and P. Hoess, "Noise performance comparison of ICCD with CCD and EMCCD cameras", in *Optical Science and Technology, the SPIE 49th Annual Meeting*, (International Society for Optics and Photonics, 2004), pp. 195–204.
32. A. Papoulis and S. U. Pillai, *Probability, Random Variables, and Stochastic Processes* (Tata McGraw-Hill Education, 2002).
33. G. Popescu, Y. Park, N. Lue, C. Best-Popescu, L. Deflores, R. R. Dasari, M. S. Feld, and K. Badizadegan, "Optical imaging of cell mass and growth dynamics," Am. J. Physiol. Cell Physiol. **295**(2), C538–C544 (2008).
34. J. Ma, L. Guo, S. J. Fiene, B. D. Anson, J. A. Thomson, T. J. Kamp, K. L. Kolaja, B. J. Swanson and C. T. January, "High purity human induced pluripotent stem cell (hiPSC) derived cardiomyocytes: electrophysiological properties of action potentials and ionic currents," Am. J. Physiol. **301**, 2006 (2011).
35. Y. A. Abassi, B. Xi, N. Li, W. Ouyang, A. Seiler, M. Watzele, R. Kettenhofen, H. Bohlen, A. Ehlich, E. Kolossov, X. Wang, and X. Xu, "Dynamic monitoring of beating periodicity of stem cell-derived

Biomedical Optics EXPRESS

cardiomyocytes as a predictive tool for preclinical safety assessment," Br. J. Pharmacol. **165**(5), 1424–1441 (2012).
36. G. M. de Peppo and D. Marolt, "State of the Art in Stem Cell Research: Human Embryonic Stem Cells, Induced Pluripotent Stem Cells, and Transdifferentiation," J. Blood Transfus. **2012**, 317632 (2012).
37. M. Ben-Ari, R. Schick, L. Barad, A. Novak, E. Ben-Ari, A. Lorber, J. Itskovitz-Eldor, M. R. Rosen, A. Weissman, and O. Binah, "From beat rate variability in induced pluripotent stem cell-derived pacemaker cells to heart rate variability in human subjects," Heart Rhythm **11**(10), 1808–1818 (2014).
38. S. Yechikov, R. Copaciu, J. M. Gluck, W. Deng, N. Chiamvimonvat, J. W. Chan, and D. K. Lieu, "Same-Single-Cell Analysis of Pacemaker-Specific Markers in Human Induced Pluripotent Stem Cell-Derived Cardiomyocyte Subtypes Classified by Electrophysiology," Stem Cells **34**(11), 2670–2680 (2016).
39. G. van den Engh and J. Visser, "Light Scattering Properties of Pluripotent and Committed Haemopoietic Stem Cells," AHA **62**, 289–298 (2008).

1. Introduction

Being able to accurately characterize human pluripotent stem cell-derived cardiomyocytes (hPSC-CMs)–cardiac muscle cells–has important applications, ranging from the development of drugs on general populations of cells or on a patient's own cells for personalized medicine [1], to classifying cells after differentiation for basic scientific studies of cardiac and stem cells and for regenerative medicine applications [2], and determining cell viability for repairing damaged heart tissue [3]. The gold standard for hPSC-CM characterization in cell culture is the whole-cell patch clamp [4], where the intracellular voltage of a cell is measured to characterize its action potential. Patch clamping is slow and tedious, is prone to user bias during cell selection, and destroys the cells after testing. A less invasive method of detecting electrical activity in cells is based on multi-electrode arrays (MEAs) to measure the extracellular field potential, but this method is not usually used for cell classification because it detects only fast transients, since it is insensitive to slow variations in cell potential [5], and it requires complex analysis to determine the origin of the signal.

Recently, less invasive optical methods of detecting and eliciting action potentials have been developed, establishing optophysiology as an alternative to electrophysiology for controlling and monitoring electrically-active cells and organs [6]. Voltage sensitive dyes and genetically encoded voltage indicators (GEVIs) change brightness of fluorescence in accordance to the transmembrane voltage. They have been used for drug testing, and have shown potential for cell classification [7, 8]. Although fluorescence techniques are less destructive and enable higher throughput than patch clamp measurements, they have other drawbacks. Voltage sensitive dyes can affect cell membrane properties and are limited by photobleaching and phototoxicity [9]. GEVIs require a lengthy process of conferring the protein expression [7].

Since cardiomyocyte motion is correlated with the action potential, as demonstrated by intracellular patch clamp measurements [10, 11] and by extracellular MEA recordings [12, 13], analysis of cell motion measured optically, herein referred to as optophysiology, could replace electrical detection. Phase microscopy enables label-free, non-destructive, and high throughput characterization of cardiomyocyte motion. Methods based on block matching, a lateral motion detection algorithm, using Zernike phase contrast microscopy have been developed to extract motion timing characteristics in dense monolayers of hPSC-CMs, such as beating frequency, regularity and duration, and changes thereof upon addition of drugs [12, 13].These methods work well on monolayers of synchronized cells, which exhibit stronger beating than single cells. Evaluation of single cell motion using lateral motion vector analysis has so far required complex manual segmentation into several slices around the origin of the beat [11]. One study demonstrated applicability of intensity correlation analysis to detection of changes in segmented blocks of images using Zernike phase contrast microscopy. It enabled detection of beating in dense monolayers and in single cells [10]. While the changes in intensity of the phase contrast images are related to a change in the cell height, analysis of the cell changes in height were not quantitative due to the nature of Zernike phase contrast microscopy [14].

Biomedical Optics EXPRESS

These methods can be improved using quantitative three-dimensional (3D) imaging of the cell shape. Quantitative phase imaging (QPI) maps the optical path difference (OPD) between the light that travels through the cell and the average path length through the sample. QPI has been used to study spatiotemporal dynamics of rat cardiomyocytes in culture [15, 16] and to analyze the temporal characteristics of strongly beating confluent, synchronized hPSC-CMs [17]. Laser-based illumination in the latter study caused speckling and out-of-focus interference, resulting in significant temporal noise. Therefore, statistical methods were necessary to extract the motion characteristics from the noisy background in populations of cells, which precluded applicability of that setup to characterization of single cells.

Previous QPI studies of other cell types demonstrated several examples of cells classification using morphological features, such as volume, dry mass, shape, and refractive index. In cancer research applications, such features have been used to classify cells as cancerous vs. noncancerous [18], discriminate between different cancer cell lines [19], and distinguish primary from metastatic cancer cells [18, 20]. QPI based morphological features can also be used to discriminate between normal and sickle cell red blood cells [21, 22], assess the effects of blood storage conditions on their shape [23], and have the potential as a marker for Parkinson's disease in neurons [24].

In this paper, we demonstrate quantitative phase imaging of cardiomyocytes with sufficiently low noise to extract timing characteristics of single asynchronously beating hPSC-CMs as well as morphological features. Using bright collimated LED illumination helps eliminate speckling and spurious interference effects associated with more coherent sources, while enabling sufficiently fast frame rates for complete characterization of the cell's beat cycle. The common path design helps minimize mechanical noise, and with the use of high optical magnification, it becomes possible to average signals over the extent of the cell to reduce the noise. Excellent signal-to-noise ratio with this method provides detailed characterization of single cells with respect to their viability, cell type, and drug interactions. This optophysiological method may not only characterize cardiomyocytes in a manner similar to traditional electrophysiology, but also enable applications that require non-invasive characterization, longitudinal follow-up, and high throughput.

2. Methods

2.1 Quantitative phase imaging system

To acquire quantitative representations of hPSC-CMs in three spatial dimensions, we employ diffraction phase microscopy (DPM) - a single shot, common-path off-axis implementation of QPI [25]. It provides a measure of optical thickness in each pixel, the optical path difference (OPD) between the cell and the average phase of the sample, which for isolated cell cultures is dominated by the medium. The OPD is defined as follows:

$$\phi(x,y) = \frac{2\pi}{\lambda}\int_0^h \left(n_1(x,y,z) - n_0\right) dz \tag{1}$$

which for a 2-dimensional representation could be simplified as following:

$$\phi(x,y) = \frac{2\pi}{\lambda}\left(n_1(x,y) - n_0\right)\cdot h(x,y) \tag{2}$$

where $n_1(x,y,z)$ is the refractive index of the sample at each point, n_0 is the refractive index of the medium, $h(x,y)$ is the height of the sample at each point, and λ is the illumination wavelength.

Unlike traditional phase microscopy techniques, which visualize morphological features of cells mostly qualitatively, QPI provides quantitative measure of the optical path length at each pixel. From this, the optical volume of the cell can be calculated as an integral of OPD over the cell area, in units of rad × μm^2. Since the OPD is proportional to the difference in

Biomedical Optics EXPRESS

refractive indices of the cell and the surrounding medium, as shown in Eq. (1-2), optical volume could be converted to cell dry mass, assuming a certain refractive increment of protein content [26], and if the reference arm provided an ideal image-free beam. However, if the reference arm in common path interferometry is not completely free of the image content, it creates a negative phase halo around the objects [27], which distorts the OPD map.

Our DPM setup, shown in Fig. 1(a), included a 660nm LED (Thorlabs M660L4) coupled into a 400 µm diameter multimode fiber and collimated by a reflective collimator (Thorlabs RC04SMA-01). The resulting beam had a divergence angle of 13 mrad. With 0.14 mW/mm^2 on the sample, the minimum time for full exposure of the camera was 8ms, matching the imaging frame rate of 125 fps. At the camera port, the beam was split by a diffraction grating (Edmund Optics 46-074) into various diffraction orders. The first order containing image information was passed through the system unaltered, and the reference arm in the common-path interferometer was obtained by filtering the zero diffraction order through a 150 micron pinhole, while the other orders were blocked. The interference pattern between the 1st and the 0th orders created on the camera after passing through the 4f system, with lenses of f_1 = 50 mm and f_2 = 250 mm, had an interference fringe width which exceeded the 2.7 pixels per fringe minimum for proper reconstruction [28]. We used two cameras in these experiments: a Basler AC2040-90-um and a Phantom v641. With the Phantom v641 camera, up to 25-30 single cells could be imaged in a field of view, depending on the plating sparsity. To reduce the mechanical noise, the entire output path was shielded from air flow.

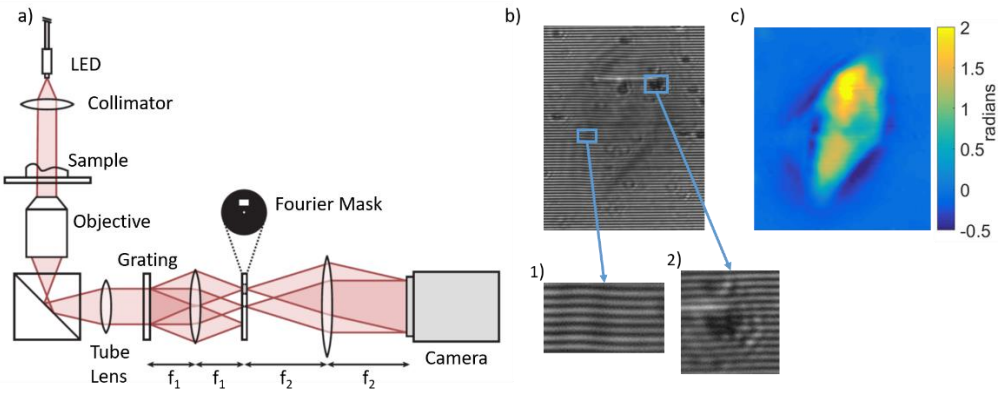

Fig. 1. a) Diffraction Phase Microscopy Setup. b) Raw image of one cell. Inset 1) Zoom illustrating bending of the diffraction fringes at the cell edge. Inset 2) Zoom illustrating dust or imperfections on the grating. c) Calculated OPD image of an hPSC-CM.

A single background image with no sample was acquired as a reference prior to cell imaging in each experiment. Fast-phase reconstruction was chosen as the preferred method to extract the OPD image and remove noise, including grating imperfections [29]. Steps taken on the sample and reference image separately included Fourier transforming the images by FFT, circularly shifting the spectrum to center the first diffraction order, applying a Gaussian low-pass filter to select the image content while rejecting the zero order, and taking the inverse FFT of the resulting images. Then the sample image was divided by the reference image, and the final OPD, excluding any static background, was calculated as the angle of the exponential function.

Further processing to extract the time-dependent changes in cells, including integration of the OPD over the cell, is described in Section 3.2. The cell area was calculated as the number of pixels within the cell boundaries, multiplied by the pixel area. The optical volume was calculated by summing the OPD over all the pixels within a cell and multiplying by the pixel area.

Biomedical Optics EXPRESS

2.2 Cardiomyocyte cell culture and imaging conditions

hPSC-CMs of type Sendai 15 [30] were differentiated from human induced pluripotent stem cells. The cells were seeded at low density and imaged in a stage top incubator at 37 °C and 5% CO_2. Only cardiomyocytes beating asynchronously with respect to neighboring cells, and without large visible vacuoles, were used for the motion analysis. A total of 116 hPSC-CM cells were analyzed from two different preparations.

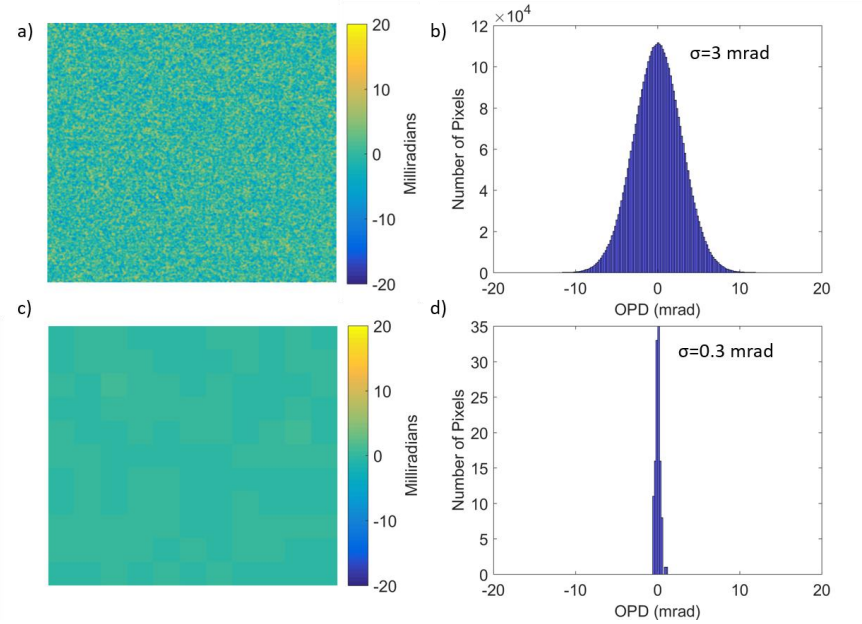

Fig. 2. a) Spatial distribution of noise in one frame. b) Histogram of the phase in pixels from a), with standard deviation noted. c) Spatial distribution of noise in one frame after spatial averaging over 173x173 pixels. d) Histogram of the phase in pixels from c), with standard deviation noted.

3. Results

3.1 Noise level in DPM system

The noise level of the imaging system defines its phase sensitivity. We characterized the spatial noise level in the processed OPD images by calculating the phase difference between sequentially acquired images without a sample. Phase distribution in the images taken with the Basler AC2040-90-um camera are shown in Fig. 2(a). The corresponding histogram, shown in Fig. 2(b), demonstrates the width of the noise distribution - 3 mrad, which is close to the shot noise level defined by the pixel well depth [31].

Integrating the phase signal over the area within the cell boundaries helps reduce the noise level. In our method of extracting the beat signal, described in Section 3.2, the phase signals in two frames are subtracted, then an absolute value is taken before summing the contributions of each pixel within the cell boundaries. Subtraction of the phase signals causes a slight increase in the standard deviation, to 4 mrad, due to summation of two independent normally distributed random variables [32]. When the signal is significantly above the noise (as in the case with cardiomyocytes in motion), taking absolute value does not change the noise distribution, and therefore the effect of averaging is similar to that in the raw noise data. A typical cell has an area between 32,000 to 600,000 pixels, with 150,000 pixels on average. Averaging over an area of 173 by 173 (about 30,000) pixels improved the noise level by an order of magnitude, as shown in Fig. 2(c)-2(d). The effect of spatial averaging is much weaker than the square root of the number of pixels due to spatial correlation introduced by

Biomedical Optics EXPRESS

the low pass filtering via pinhole and by the spatial frequency cut-off during image reconstruction.

For pixels with the signal near the noise level, the absolute value operation converts the noise distribution into a half normal, resulting in an offset of the average by $\sigma\sqrt{(2/\pi)}$, where σ is the standard deviation of the normal distribution before the absolute value operation [32]. This offset by about 3 mrad per pixel in the absence of signal results in a small positive value of the phase rate of change during the rest periods, as shown below (Fig. 4(a)).

Conversion of the phase sensitivity into minimum detectable motion depends on the difference in refractive indices between the cell and the surrounding medium. Rearranging Eq. (2) to express Δh as a function of $\Delta\phi$ yields the following:

$$\Delta h(x,y) = \frac{\lambda \Delta\phi(x,y)}{2\pi\left(n_1(x,y) - n_0\right)} \tag{3}$$

with λ = 660 nm, and the minimum refractive index difference n_1-n_0 = 0.05 [33], 3 mrad of phase noise corresponds to about 6nm of motion.

Temporal noise in the system was measured by acquiring 300 frames, with no sample. Using the first frame as a reference, the standard deviation of the phase value in each pixel over time turned out to be 1.8 mrad. Averaging the phase value in each pixel over multiple frames decreased the noise level by the square root of the number of frames, as expected for a white Gaussian noise.

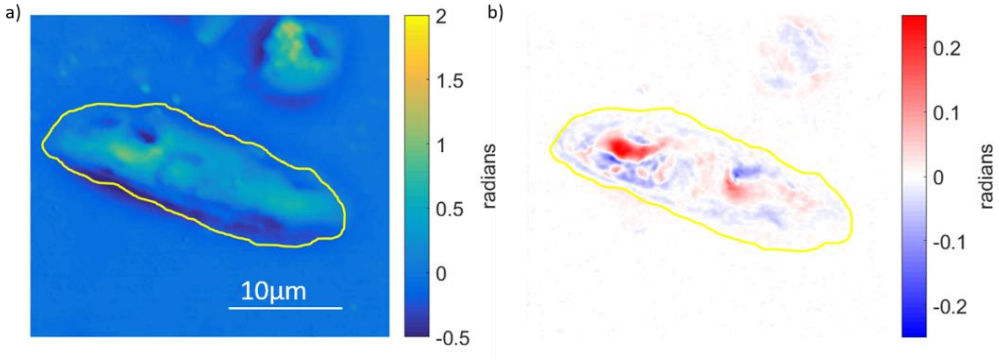

Fig. 3. a) Phase image of a cell with outlined boundaries. b) Maximum changes in phase during the beating cycle.

3.2 Analysis of the cell motion

hPSC-CMs are typically characterized by the shape of their action potentials [34]. Since motion of the cardiomyocytes is controlled by the changes in cell potential [12], we analyze the cell motion instead.

An example of a phase image of a cardiomyocyte, relative to the sample-free reference is shown in Fig. 3(a). Cell beating can be seen in a time-series of such images, as shown in a video Visualization 1. Cell movements can be seen better when subsequent images are subtracted from the first frame, as shown in Fig. 3(b), and in the video Visualization 2, where an increase in optical thickness is shown in red, and a decrease - in blue. With the phase changes during beating cycles reaching 200-300 mrad, and noise level of about 3 mrad, the SNR is on the order of 100:1.

The phase rate of change ($d\phi(x,y)/dt$) is then calculated in each pixel for each time point using the following relationship:

Biomedical Optics EXPRESS

$$\frac{d\phi(x,y)}{dt} = \frac{\left(\phi_{+1}(x,y) - \phi_{-1}(x,y)\right)}{2} \times r \tag{4}$$

where $\phi_{-1}(x,y)$, $\phi(x,y)$ and $\phi_{+1}(x,y)$ are the measured OPD at one pixel, in three consecutive frames, and r is the frame rate of the camera.

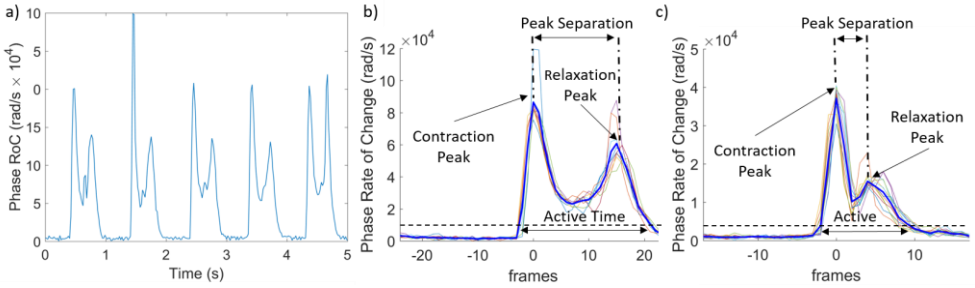

Fig. 4. a) Phase rate of change calculated from the time-dependent data in Fig. 3. b) Characteristic beat cycle of cell in a). c) Example of the phase rate of change data from another cell, showing variation between cells.

One way to assess cell dynamics is to integrate the phase rate of change over the cell. For this purpose, the cell boundaries are first defined using ImageJ, as illustrated in Fig. 3, and a binary mask with all cells in the field of view is created. Absolute values of the phase rate of change for each frame, given in Eq. (4), are calculated for every pixel in the cell and then summed over all pixels within the cell boundary, collapsing the data into a single value per time point for a cell. This data can be plotted over time as shown in Fig. 4(a), where two peaks in the periodic signal represent the contraction and relaxation parts of the beating cycle. SNR in this approach exceeds 100:1.

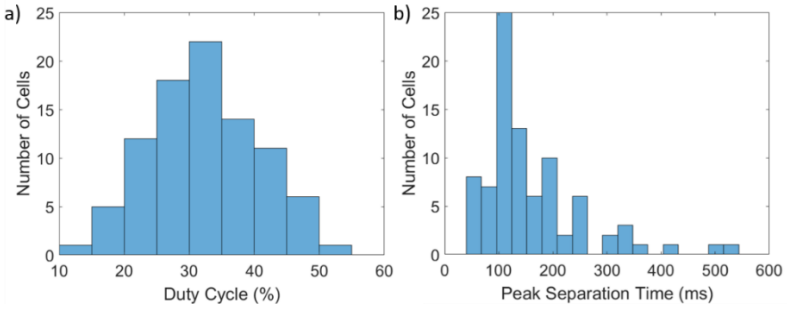

Fig. 5. Distributions of selected characteristic cycle parameters in population of cells. a) Duty cycle. b) Peak separation time.

3.3 Characteristic beating cycles

To extract a characteristic beating cycle for each cell, the peaks of the phase rate of change are identified, overlaid, and the cycles are averaged together. Examples of characteristic cycles of two different cells are shown in Figs. 4(b)-4(c) in bold, while the individual cycles are shown on the same scale with thinner lines. Characteristics of the cell dynamics, such as peak separation (delay between the contraction and relaxation peaks) and the active time (phase rate of change above certain threshold), can be extracted from the average cycle, as demonstrated in Figs. 4(b) and 4(c). Threshold phase rate of change for the definition of the active time was set to 15% of the peak value.

The hPSC-CMs are typically classified into atrial-, nodal-, and ventricular-like subtypes [34], based on the shape of AP. The action potential duration (APD) is often defined as a

Biomedical Optics EXPRESS

length of the plateau at 80-90% level of the maximum, corresponding to the time between the contraction and relaxation phases of the beating cycle. The peak separation in the phase rate of change plot represents a similar characteristic. The active time was chosen as a parameter that may be related to the lower threshold (10-20%) of the APD. Histograms in Fig. 5 show the distribution of the peak separation time and of the duty cycle, calculated as the fraction of the active time within the total cycle duration.

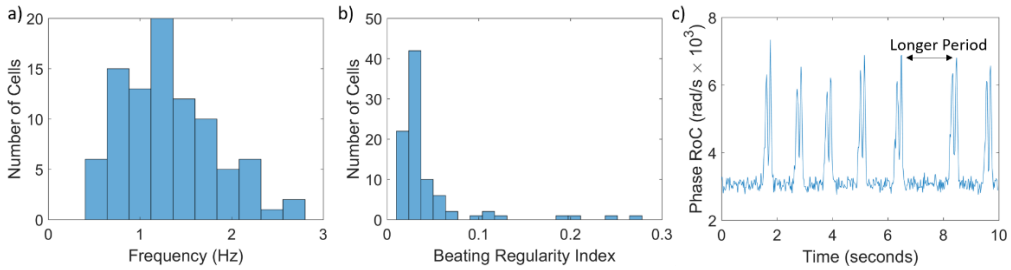

Fig. 6. a) Histogram of the average frequency for 90 cells. b) Histogram of BRI for 90 cells. c) Example of irregularly beating cell representing higher end of the BRI spectrum.

3.4 Quantifying cellular activity

Beating frequency is an important parameter in classifying cell types and characterizing their responses to drugs [2, 35, 36]. Frequency was calculated as the inverse of the average beat period, and the distribution of frequencies among the cell population is shown in Fig. 6(a). Irregular beating of single nodal hPSC-CMs has been linked to irregularity in the heart beat [37], and is an important indicator of drug toxicity [35]. The Beat Regularity Index (BRI), defined as the standard deviation of the beat period divided by the mean beat period, was calculated for 90 cells and its histogram is shown in Fig. 6(b), where irregular cells, such as the one shown in Fig. 6(c), represent higher values in the histogram.

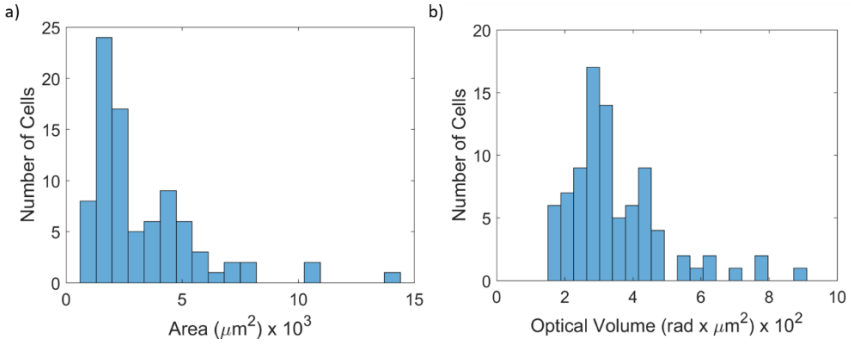

Fig. 7. The area (a) and optical phase volume (b) in a population of cells.

3.5 Cardiomyocyte shape characteristics

One potentially important factor for cell classification is their size. Distributions of the area and optical phase volume in a population of hPSC-CMs are shown in Fig. 7. The average area was 3223 ± 2394 μm^2, ranging from 720 to 14299 μm^2. The average optical phase volume was 349 ± 141 rad × μm^2, ranging from 155 to 891 rad × μm^2. Monitoring these characteristics over time would provide a quantitative measure of cell growth or decline under various environmental conditions, and the differences in size of hPSC-CMs may be used for their classification.

Biomedical Optics EXPRESS

4. Discussion

QPI with bright collimated LED illumination provides quantitative measures of the cell motion with low noise, thereby enabling analysis of the dynamics of single asynchronously beating cells, rather than the confluent beating populations analyzed previously with significantly noisier QPI [17]. Axial integration of the optical phase makes this method more inclusive and more sensitive than lateral motion vector detection methods, including block detection [11–13]. Previously reported Zernike methods have SNR in the range of 10:1 to 40:1 on populations of beating cells, and SNR greatly decreases with weakly beating single cells.

Analysis of the cell-integrated rate of phase change reveals the peaks corresponding to contraction and relaxation of the beating cell, similar to observations based on Zernike phase contrast methods in confluent populations of cells, where timing of several aspects of the motion signal has been correlated with different parts of the action potential. Such correlation could replace tedious and destructive patch-clamp recordings (electrophysiology) with non-invasive quantitative phase imaging (optophysiology).

Histograms of all characteristics of the beating cycle analyzed with our method, including beating frequency, active time and duty cycle, showed a continuous distribution of properties. Although traditionally hPSC-CMs are classified into the atrial-, nodal-, and ventricular-like subtypes, recent studies demonstrated that hPSC-CMs do not cleanly separate into these classes, and their properties represent a continuum, changing over time [2, 38]. Our data supports this conclusion and enables observation of their development over time. One particularly useful measure of cells' health is regularity of their beating cycle [34, 37]. This measure is quantified by the Beating Regularity Index (BRI) histogram, which can be easily extracted from QPI data, and used for assessment of the cell viability and drug testing. Monitoring the phase variation during beating cycle, based on either the absolute maximum or the average phase change over a cell, may provide a convenient quantitative measure of cell activity, for which currently there is no established metric.

Light scattering properties related to cell size and shape were used to classify pluripotent and differentiated hematopoietic stem cells with flow cytometry [39]. Similarly, cell optical phase volume may be helpful for classification of hPSC-CMs. QPI-based optical phase volume measurement may be advantageous compared to other methods of volume characterization, such as confocal microscopy, because dry mass is insensitive to variations in osmolarity [33], and data can be acquired in a single shot. QPI measurements can also be performed while the cells are attached to a surface and beating, unlike flow cytometry.

5. Conclusions

QPI enables a non-invasive, label-free method for analysis of cell size, shape and motion, with high SNR. Optophysiology using QPI provides a non-destructive and simple alternative to classical patch-clamp based electrophysiological characterization of cardiomyocytes. QPI detects the beating cycle, with its characteristic contraction and relaxation phases, and can be used for longitudinal analysis of the stem cells' development for utilization in regenerative medicine. It can also be used for development of drugs, including personalized medicine applications.

Since patch clamp affects cell motion, it impedes direct comparison of the action potential with motion in single cells, and therefore less invasive measurements of cell potential are required. One such method could be voltage-sensitive dyes, and further studies may shed additional light relating the details of cell motion to dynamics of its electric potential.

Biomedical Optics EXPRESS

Funding

National Institutes of Health (NIH) (U01 EY025501, OJA supported by K01 HL130608); Stanford Vice Provost for Graduate Education (CEC supported by DARE Fellowship); Stanford Neurosciences Institute (GG supported by Interdisciplinary Scholars Award).

Acknowledgements

We thank Nathan Loewke for helpful discussions on image processing and algorithm design. We thank Yi Quan for her help with cell culture.

Disclosures

The authors declare that there are no conflicts of interest related to this article.